Comparison between a 2.5 MW DFIG and CDFIG in Wind Energy Conversion Systems

H. Dehnavifard, X. M. Hu, and M. A. Khan, P. S. Barendse

Abstract— **A 2.5MW doubly-fed induction generator (DFIG) and a cascade doubly-fed induction generator (CDFIG) in energy conversion system are compared in order to investigate the cost and efficiency of the system. A reference doubly-fed induction generator and a scaling methodology are employed to design the cascade doubly-fed induction generator Using finite element analysis (FEA) and MATLAB/Simulink, both doubly-fed induction generator and cascade doubly-fed induction generator are modeled under similar wind profiles. The total active and reactive output power for both generators are presented. The efficiency of the cascade doubly-fed induction generator is better than the doubly-fed induction generator, however, this is only notable in large scale wind energy generation.**

Index Terms— **Cascade-DFIG, DFIG, design, efficiency, scaling, and wind energy.**

I. Introduction

In recent decades, there has been an increase in renewable energy penetration in the grid. Wind Energy Conversion Systems (WECS) are a more attractive form of renewable energy because of their low cost [1], [2]. Doubly-fed induction generators (DFIGs) is employed in WECS due to their lower cost advantages over other types of generators. However, gear box and slip rings maintenance are the major problems this system (WECS with DFIG) [3], [4]. Thus, cascaded double-fed induction generator (CDFIG) also known as double stator induction generators is proposed as an attractive alternative for WECS [5]–[7]. CDFIGs are formed from two DFIGs which are connected mechanically and electrically, but are uncoupled magnetically. CDFIGs have the DFIGs' advantages plus less maintenance cost for slip rings and gears. In fact, CDFIG with enough DFIGs can drive gearless if it could be controlled. Also, the parasitic torque is not a challenge for CDFIGs against permanent magnet synchronous generators [8]–[10]. The objective of this paper is to investigate the impact of CDFIGs versus DFIGs in order of cost and efficiency. Therefore, a reference DFIG is employed and CDFIG by using scaling methodology is designed. The CDFIG will behave the same as reference DFIG under transient condition, but with different structure.

The WECS components are modeled and the losses are analyzed in the next section. Thereafter, the scaling methodologies are presented and the reference DFIG is adapted. The reference DFIG and scaled-DFIG are verified. Transient models of the CDFIG and DFIG are introduced to simulate them in MATLAB/Simulink in the third section. Lastly, the simulation results are illustrated and discussed.

H. Dehnavifard is with the Department of Electrical Engineering at University of Cape Town, (e-mail: dhnhos001@myuct.ac.za).

X. M. Hu is with the Department of Electrical Engineering at University of Cape Town, (e-mail: mason.hu@alumni.uct.ac.za).

M. A. Khan is with the Department of Electrical Engineering at University of Cape Town, (e-mail: : azeem.khan@uct.ac.za).

P. S. Barendse is with the Department of Electrical Engineering at University of Cape Town, (e-mail: paul.barendse@uct.ac.za).

II. Wind Turbine Power Analysis

The power curve of a 2.5 MW wind turbine manufactured by Vestas is employed. Fig. 1 shows the power captured by this generator and table I presents the turbine properties [11]. The rotor speed is controlled by the pitch controller in the high wind speed region not to exceed 25 (m/s).

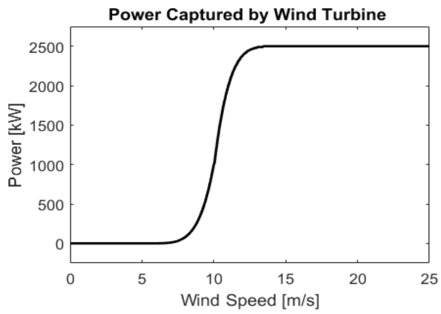

Fig. 1. Power captured by wind turbine versus wind speed.

TABLE I
2.5 MW Vestas wind turbine properties.

Vestas WECS Properties	
Operating DATA	
Rated Power [MW]	2.5
Operating Temperature [$^\circ C$]	-20 to 40
Rotor	
Rotor Diameter [m]	100
Swept Area [m^2]	7854
Nominal Revolutions of Turbine [rpm]	13.37
Electrical	
Frequency [Hz]	50
Generator Type	DFIG / CDFIG
Gearbox	
Type	Two Planetary Stages
Blade Dimension	
Length [m]	49
Maximum Chord [m]	3.9

The wind power captured (P_{wind}) by wind turbine can be calculated as follow:

$$P_{wind} = \frac{1}{2}\,\rho\, A\, C_p\, V^3 \quad (1)$$

$$\lambda = \frac{\Omega\, R_{radius}}{V} \quad (2)$$

$$C_p = a_0 + a_1\lambda + a_2\lambda^2 + a_3\lambda^3 + a_4\lambda^4 + a_5\lambda^5 + a_6\lambda^6 \quad (3)$$

where ρ is air mass density, A is rotor blades swept area, C_p is power coefficient, λ is tip-speed ratio, V is wind speed, Ω

978-1-5090-2538-1/16/$31.00 ©2016 IEEE

is turbine's rotor angular velocity and R_{radius} is the turbine's blade radius. Also a_0, a_1, a_2, a_3, a_4, a_5 and a_6 are wind characteristic coefficients.

III. Drivetrain Modeling

Two planetary stages and a helical stage gearbox are assumed to be used in this paper throughout. The gearbox weight can be computed by the shaft torque and gear ratio as follows [12]–[14]:

$$G_{gear} = 3.2\frac{T_m F_w F_s}{1000} \tag{4}$$

where T_m is the output torque of gearbox (N/m), F_w is the weight factor and F_s is the service factor. The weight factor is given in (5):

$$F_w = \frac{1}{Z} + \frac{1}{Z\, r_w} + r_w + r_w^2 + 0.4\frac{1+r_w}{Z} \times (r_{ratio} - 1)^2 \tag{5}$$

where Z in the number of planet wheel in the each stage; the wheel ratio $r_w = \frac{r_{ratio}}{2} - 1$, where "r_{ratio}" is the two planetary stages gear ratio.

IV. WECS Loss analysis

The various losses considered in WECS are illustrated in Fig. 2.

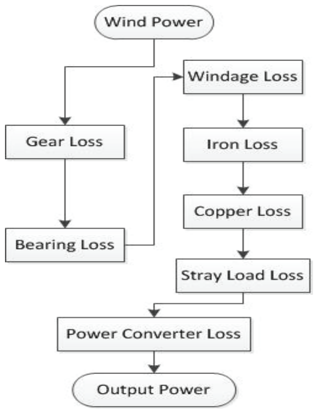

Fig. 2. Losses in WECS with DFIG

A. Mechanical losses

Gear loss (P_{Gear}) is the friction among gears in a gearbox when it transfers torque from the turbine to the generator. Bearing loss (W_b) and windage loss (W_w) are other mechanical losses in WECS. Mechanical losses are calculated using equations (6-8), where K_B is the bearing loss coefficient and K_W is the windage loss coefficient. The wind power minus the mechanical losses is input power to the generator [15]. Here, the bearing and gear losses are assumed constant for both systems and their windage losses are neglected.

$$P_{Gear} = P_{Gream}\frac{n}{n_{rated}} \tag{6}$$

$$W_b = K_b \omega_m \tag{7}$$

$$W_w = K_w {\omega_m}^2 \tag{8}$$

where P_{Gearm} is the gearbox loss at rated speed, n is rotational speed, n_{rated} is the rated rotational speed, and ω_m is angular speed.

B. Iron Loss

The iron loss includes hysteresis loss and eddy-current loss. These are calculated through equations (9-11), where K_1 is hysteresis coefficient, K_2 is eddy-current coefficient, E_0 is the reference voltage, E' is the voltage, B_0 is the reference flux density, and W is iron core weight [15], [16].

$$W_i = W_h + W_e = K_1 f B^{1.6} + K_2 f^2 B^2 \tag{9}$$

$$B = B_0 \frac{E'}{E_0} \tag{10}$$

$$r_m = \frac{{E'}^2}{W_i.\frac{W}{3}} \tag{11}$$

C. Copper Loss

Copper losses are calculated using equivalent circuit parameters.

$$P_s = R_s.{I_s}^2 \tag{12}$$

$$P_r = R_r.{I_r}^2 \tag{13}$$

where, P_s and P_r are stator and rotor copper losses, R_s is the stator resistance, R_r is the rotor resistance, I_s is the stator current and I_r is the rotor current.

D. Stray Load Loss

Stray load loss can be calculated by equation (14), where P_R is the rated power of the generator and P is the output power of the generator.

$$W_s = 0.005\,\frac{P^2}{P_R} \tag{14}$$

E. Converter Loss

Switching losses and conducting losses are usually taking to as converter losses. The switching losses of the transistors are the turn-on and turn-off losses. For the diode the switching losses mainly consist of turn-off losses, i.e., reverse-recovery energy. The turn-on and turn-off losses for the transistor and the reverse-recovery energy loss for a diode can be found from data sheets. The conducting losses arise from the current through the transistors and diodes. The converter losses is assumed the same for DFIG and CDFIG.

V. Analytical Design and Scaling Methodology

A. Electrical Machine Design Algorithm

The induction machine (IM) design algorithm is shown in Fig. 3 [17]. The design process is usually started by choosing electric and magnetic loadings according to machine specifications such as rated-power, rated-voltage, frequency, etc. It is also required to assume the current densities and the flux densities at the same time. By referring to assigned parameters, conductors' and cores' cross section area as well as slot's and tooth's dimensions are calculated in (2) and then they are adjusted in (3). After the geometrical data verified in (4), magnetic current, equivalent circuit parameters, slip and losses are respectively computed in the next 3 steps. Power factor, starting current, temperature rise and breakdown torque are calculated in (8). The design process will be finalized if the machine performance parameters are satisfactory.

B. Scaling Methodology

Due to have similar behaviors, the scaling process is used to design CDFIG. Therefore, it is possible to compare them based on cost and efficiency while there are no other benefits to distinguish one is better than the other. There are several methods that have been developed to scale electrical machines [18]. In [19], the authors indicate scaling factors which represent the scaled-machine properties and the network dynamic model.

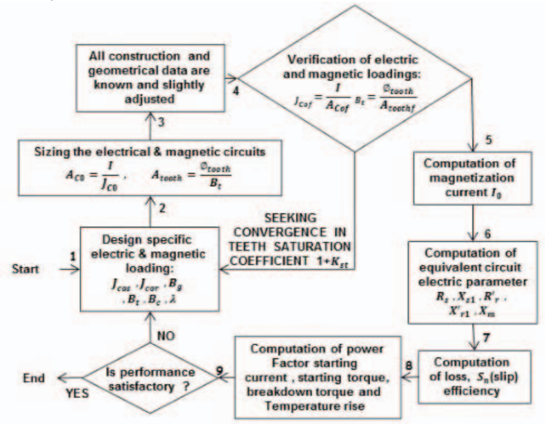

Fig. 3. The induction machine design algorithm

In [20], the design of a micro-alternator is presented, where negative-resistance is used to obtain representative constants of the model's rotor circuits. The results show a strong effect on the losses in the scaled model. A novel micro-machine model is introduced in [21] which adjusts eight of the transient and sub-transient characteristic time constants of a double fed machine (DFM). The difficulty with geometric scaling methods introduced earlier is the resulting flux density and current density in the micro-machine is low. In [22], the authors propose a simple scaling process to design new machines using the details of similar existing machines. This process was applied to the design of an induction machine which resulted in ratings that are not too far from the reference machine ratings.

In this paper, a 2.5 MW, 690 V, 4 pole machine in [23] is the reference. Table II shows the scaling equations while table III indicates the analytical specifications for both reference and scaled DFIGs [22]. Voltage, flux densities and current density are assumed constant. The power is scaled to 1.25 MW and also losses are minimized through down-scaling to keep the efficiency.

TABLE II
THE SCALING RELATIONS

Parameter	Symbol	Relation ($\frac{P_{scale}}{P_{ref.}}$)	No.
Power	$P \propto V.I$	$k_l.k_D{}^3$	(16)
Losses	$Loss \propto R.I^2$	$k_l.k_D{}^2$	(17)

The relations of powers and losses are expressed in equation (16-17), where k_L is the length factor and k_D is the diameter factor. The DFIG and scaled-DFIG analytical specifications are verified in Maxwell 2D and Fig. 4a and 4b show their flux and current densities. Due to material consumption has direct impact on the cost of the machines and alternating materials' price in the market, table IV just presents the material consumption for DFIG and CDFIG. As shown, CDFIG uses less copper than DFIG and it also is slightly lighter in core. Although, CDFIG casing and manufacturing would be more expensive, CDFIG's material is less expensive.

VI. GENERATORS MODELING

Machine behaviors during steady-state can be accurately presented by a conventional steady-state model derived in various literatures. However, this model does not cater for the dynamic behavior of the machine during its transient operations.

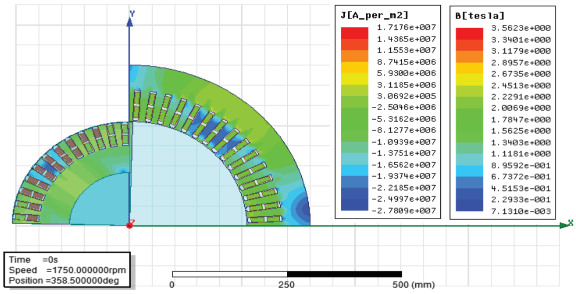

(a)

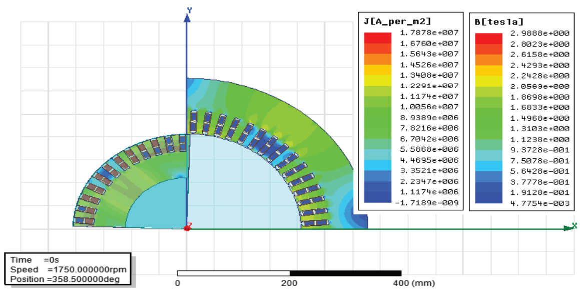

(b)

Fig. 4. The flux and current densities in a) 2.5 MW and b) 1.25 MW DFIGs

TABLE III
ANALYTICAL DETAILS OF DFIG AND CDFIG

Analytical Design Results		DFIG	Scaled DFIG
Power [MW]		2.5	1.25
Efficiency [%]		93	93
Stator number of turn		240	360
Rotor number of turn		480	576
Voltage [V]		690	690
Stator Current [A]		2420	837
Torque [N.m]		13270	6635
Construction Details			
Airgap [mm]		1.6	1.3
Outer Diameter [m]		0.8	0.655
Stator Diameter [m]		0.52	0.413
Shaft Diameter [m]		0.2663	0.222
Core Length [m]		0.52	0.413
Stator Slot [m]	width	0.0136	0.0108
	height	0.0688	0.0433
Rotor Slot [m]	width	0.0152	0.0121
	height	0.052	0.032
airgap flux density [T]		0.75	0.75
Stator flux density [T]	core	1.55	1.55
	teeth	1.5	1.5
Rotor flux density [T]	core	1.6	1.6
	teeth	1.735	1.79
Equivalent Circuit Parameters			
Stator resistance [p.u.]		0.0182	0.0239
Stator leakage inductance [p.u.]		0.347	0.39
Rotor resistance [p.u.]		0.04	0.05
Rotor leakage inductance [p.u.]		0.402	0.405
Magnetization inductance [p.u.]		10.85	9.83

Using reference frame theory, different machines can be modelled dynamically with appropriate reference frame orientation. This section will first detail the modelling process for a single DFIG. The CDFIG dynamic model will be partially based on the single DFIG model.

TABLE IV
MATERIAL CONSUMPTION IN DFIG AND CDFIG

Materials	DFIG	CDFIG
Cores (Silicon-Steel) [kg]	1320.6	1265
Windings (Copper) [kg]	448.4	338

A. DFIG Modeling

To start with the modelling process, the machine is determined to be a wound rotor induction machine. This machine has three phase start-connected windings for both stator and rotor. The rotor windings are connected to external contacts which permits access to the rotor voltages and currents. These rotor voltages and currents can be controlled to produce magnetic field inside the machine, which allows the machine to operate in sub-synchronous speed or super-synchronous speed during generating mode or motoring mode [24], [25]. The voltage and flux equations of the machine in the synchronous $d-q$ reference frame can be expressed through equations (18-21).

$$V_s = R_s i_s + \frac{d}{dt}\varphi_s + j\omega_s\varphi_s \tag{18}$$

$$V_r = R_r i_r + \frac{d}{dt}\varphi_r + j(\omega_s - \omega_r)\varphi_r \tag{19}$$

$$\varphi_s = L_s i_s + L_m i_r \qquad L_s = L_{ls} + L_m \tag{20}$$

$$\varphi_r = L_m i_s + L_r i_r \qquad L_r = L_{lr} + L_m \tag{21}$$

Where, V_s and V_r are stator and rotor voltage, i_s and i_r are stator and rotor currents, φ_s and φ_r are stator and rotor fluxes R_s and R_r are stator and rotor winding resistances, L_s and L_r are stator and rotor self-inductances, L_{ls} and L_{lr} are stator and rotor leakage-inductances, L_m is the machine's mutual inductance and ω_s and ω_r are machine's synchronous and rotor speed. The mechanical equations of the machine can also be expressed with respect to fluxes, currents and the machine inertia.

$$T_e = \frac{3}{4}P\left(\frac{L_m}{L_s}\right)\left(\varphi_{qs}i_{dr} - \varphi_{ds}i_{qr}\right) \tag{22}$$

$$\frac{d}{dt}\omega_m = (T_e - T_m)\frac{P}{2J} \tag{23}$$

The voltage, current and flux of the machine can be expressed in terms of $d-q$ axes components, which are indicated by subscripts d and q. The transformation between machine three-phase abc quantities and $d-q$ quantities is performed by using Parke's transformation defined in equation (24).

$$\begin{bmatrix} V_d \\ V_q \\ V_o \end{bmatrix} = \sqrt{\frac{2}{3}}\begin{bmatrix} \cos(\theta) & \cos(\theta - \frac{2\pi}{3}) & \cos(\theta + \frac{2\pi}{3}) \\ \sin(\theta) & -\sin(\theta - \frac{2\pi}{3}) & -\sin(\theta + \frac{2\pi}{3}) \\ \frac{\sqrt{2}}{2} & \frac{\sqrt{2}}{2} & \frac{\sqrt{2}}{2} \end{bmatrix}\begin{bmatrix} V_a \\ V_b \\ V_c \end{bmatrix} \tag{24}$$

Under the assumption that the stator and rotor of the machine are connected to an ideal balanced grid, the component V_o can be neglected since $V_a + V_b + V_c = 0$. By neglecting the stator resistance due to its lack of impact on the grid voltage, and knowing that the machine is modelled in the flux-oriented synchronous reference frame, the following conditions for the stator voltage and flux holds true:

$$\begin{bmatrix} \varphi_{ds} \\ \varphi_{qs} \end{bmatrix} = \begin{bmatrix} |\varphi_s| \\ 0 \end{bmatrix} \tag{25}$$

$$\begin{bmatrix} V_{ds} \\ V_{qs} \end{bmatrix} = \begin{bmatrix} 0 \\ |V_s| \end{bmatrix} \tag{26}$$

These conditions give rise to equations (27-29) with respect to the machine power and electromagnetic torque:

$$T_e = \frac{3}{4}P\left(\frac{L_m}{L_s}\right)(-\varphi_{ds}i_{qr}) \tag{27}$$

$$P_s = -V_{qs}\left(\frac{L_m}{L_s}\right)i_{qr} \tag{28}$$

$$Q_s = \frac{V_{qs}^2}{\omega_s L_s} - \frac{V_{qs}L_m}{L_s}i_{dr} \tag{29}$$

Where, P_s and Q_s are the stator active and reactive power. It can be noted that, since the machine is connected to a balanced grid, the stator flux remains constant during steady-state. By observing the above equations, it can be seen that the electromagnetic torque is directly proportional to the q-axis component of the rotor current. The active and reactive power of the stator can be controlled directly by q-axis and d-axis rotor current, respectively. The above dynamic equations of the machine can be used as the basis for machine controller design, and can be implemented in simulations using MATLAB/Simulink.

B. CDFIG Modeling

1) Operation principles of CDFIG

Fig. 5 below presents the schematic of a CDFIG.

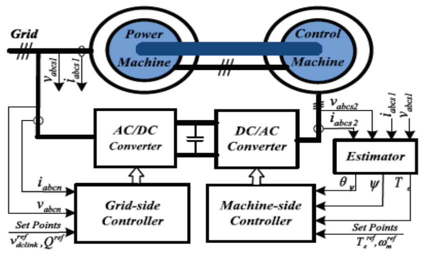

Fig. 5. Configuration of the CDFIG

The machine consists of two DFIGs coupled through the rotor both mechanically and electrically. The power machine, which is directly connected to the grid through its stator, is responsible for exchanging main power flow with the grid. The control machine, which is connected to the grid via a back-to-back AC converter, is responsible for adjusting the rotor speed by controlling its stator voltage [26], [27]. The electrical interconnection of rotors between the two DFIGs can be either direct connection with similar phase sequence, or inverse connection. These two types of connections can be denoted as an integer variable α where, direct coupling ($\alpha = 1$) and inverse coupling ($\alpha = -1$) [28]. It is shown in literature that for higher machine efficiency, the CDFIG must be operated in inverse coupling mode. Now considering the mechanical coupling between the two DFIGs, the mechanical speed of the CDFIG can be expressed as:

$$\omega_m = \frac{\omega_{s1} - \alpha\omega_{s2}}{P_1 - \alpha P_2} \tag{30}$$

where, ω_{s1} and ω_{s2} are synchronous speed of the power machine and control machine respectively, P_1 and P_2 are number of pole pairs for the power machine and control machine respectively. The natural speed of the rotor, ω_n, is defined as the rotor mechanical speed when $\omega_{s2} = 0$.

2) Dynamic model of CDFIG

The CDFIG model can be derived based on the single DFIG dynamic equations. However, it is important to consider the relative speed between the power and control machine reference frames. In this paper, subscript 1 and 2 will indicate variables that belong to the power and control machine respectively. Fig. 6 shows the relative speed between different reference frames of the power and control machine [29]. The CDFIG in this paper is modelled dynamically in the synchronous $d-q$ reference frame of the power machine. Furthermore, the two DFIGs are identical with an inverse electrical coupling between their rotor windings. Hence the voltage equations for the CDFIG can be expressed as:

$$V_{s1} = R_{s1} i_{s1} + \frac{d}{dt}\varphi_{s1} + j\omega_{s1}\varphi_{s1} \quad (31)$$

$$V_{s2} = R_{s2} i_{s2} + \frac{d}{dt}\varphi_{s2} + j[\omega_{s1} - (P_1 + P_2)\omega_m]\varphi_{s2} \quad (32)$$

$$V_{r1} = R_{r1} i_{r1} + \frac{d}{dt}\varphi_{r1} + j(\omega_{s1} - P_1\omega_m)\varphi_{r1} \quad (33)$$

$$V_{r2} = R_{r2} i_{r2} + \frac{d}{dt}\varphi_{r2} + j(\omega_{s1} - P_2\omega_m)\varphi_{r2} \quad (34)$$

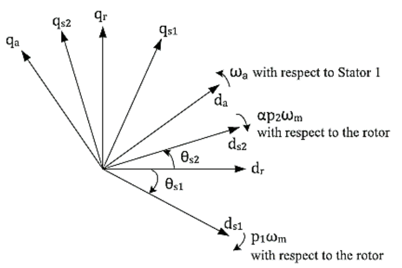

Fig. 6. Vector diagram of CDFIM reference frames.

Since the rotor is connected electrically, the rotor voltage equations can be combined by noting the rotor connection constraints where, $V_{r1} = V_{r2}$ and $i_{r1} = -i_{r2} = i_r$. Thus the combined rotor voltage equation can be expressed as:

$$V_r = V_{r1} - V_{r2} = R_r i_{r1} + \frac{d}{dt}\varphi_r + j(\omega_{s1} - P_1\omega_m)\varphi_r = 0 \quad (35)$$

where R_r, V_r, φ_r are all combined rotor values that represent the rotor in a common perspective.

$$R_r = R_{r1} + R_{r2} \quad (36)$$

The flux linkage equations for the CDFIG are:

$$\varphi_{s1} = L_{s1} i_{s1} + L_{m1} i_r \quad (37)$$

$$\varphi_{s2} = L_{s2} i_{s2} + L_{m2} i_r \quad (38)$$

$$\varphi_r = L_{m1} i_{s1} + L_r i_r - L_{m2} i_{s2} \quad ; \quad L_r = L_{r1} + L_{r2} \quad (39)$$

The mechanical model of CDFIG can be modelled by torque and inertial equations similar to the model of the single DFIG. However, the electromagnetic torque generated by the machine is expressed as the sum of individual machine torques.

$$T_e = \frac{3}{2} P_1 L_{m1}\left(i_{qs1} i_{dr} - i_{ds1} i_{qr}\right) + \frac{3}{2} P_2 L_{m2}\left(i_{ds2} i_{qr} - i_{qs2} i_{dr}\right) \quad (40)$$

$$\left(\frac{J_1 + J_2}{P_1 + P_2}\right)\frac{d}{dt}\omega_m = T_e - T_m \quad (41)$$

The above dynamic equations in the synchronous frame of the power machine describe the complete system, both electrically and mechanically. This model can then be implemented in simulation software for analysis.

VII. Simulation Results

The wind profile used is shown in Fig. 7.

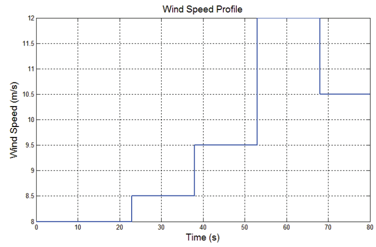

Fig. 7. The assumed wind speed profile

The machine will generate 2.5MW at the rated speed of $12m/s$. The wind speed changes initially at t = 23s, thereafter each subsequent variation is a step in wind speed, which simulates the worst case scenario of wind speed variation. Based on this wind speed profile, simulations for both DFIG and CDFIG were conducted for a total duration of 80s. The control is based on the stator-flux-oriented vector control principles. Fig. 8 shows that the stator voltage and frequency evidently are constant and also equal due to their connection to the grid.

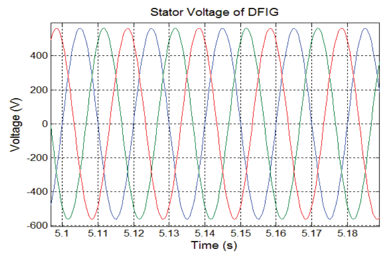

Fig. 8. The stator voltage versus time for both machines.

A. DFIG Results

The stator current is indicated in Fig. 9.

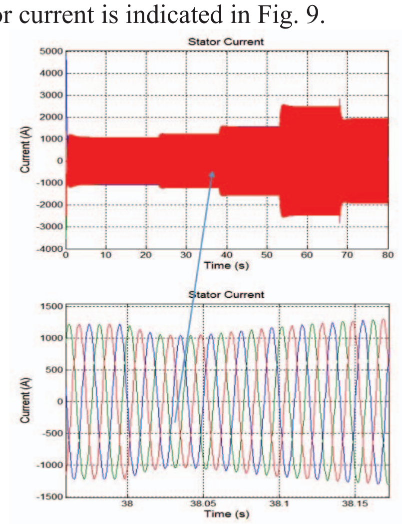

Fig. 9. The DFIG stator output current

Its magnitude varies based on input power and it is at rated value between 53 and 68 seconds. The rotor voltages are the control inputs to the DFIG. It varies in magnitude and frequency depending on the rotor speed which in turn is commanded by the maximum power point tracking (MPPT) algorithm. The rotor speed is indicated in Fig. 10.

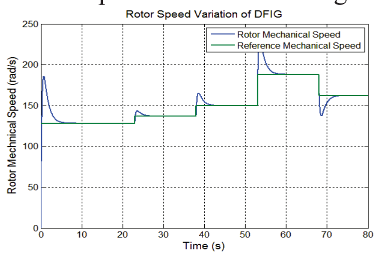

Fig. 10. The DFIG rotor speed

The control system ensures that any change in rotor speed will settle to steady-state within 4s. The speed of the DFIG corresponding to the rated power is $188rad/s$ which is 1.2 p.u. of synchronous speed. With varying wind speed, the rotor speed of the generator was controlled to achieve maximum power point tracking. Fig. 11a shows the stator active and reactive power. The stator reactive power is controlled to be 0 for unity power factor operation on the DFIG stator. The active power varies with changing rotor speed since there is a cross relation between the rotor speed and output power of the machine through MPPT. The values are negative due to the motoring machine modelling convention, this shows that the stator is always delivering active power to the grid whether in super-synchronous or sub-synchronous mode. The rotor active and reactive power is a fraction of the stator power as seen from Fig. 11b.

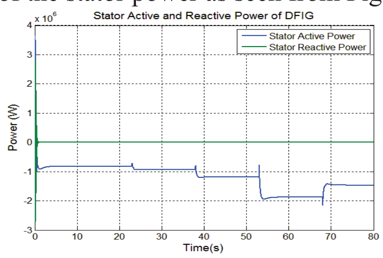

a)

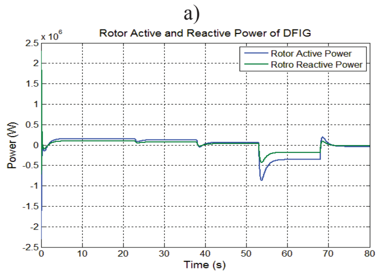

b)

Fig. 11. The DFIG a) stator active and reactive power and b) rotor active and reactive power.

Up until 53s, the machine is in sub-synchronous mode, hence rotor power transfer from grid to the machine. Between 53 and 68 seconds, the machine is in super-synchronous mode hence power transfer from machine to grid. Between 68 and 80 seconds, the machine is operating close to the synchronous speed hence rotor power is almost 0. The DFIG input mechanical power and total output power are illustrated in Fig. 12. By comparing the input and output power of the DFIG, the average efficiency of the machine is calculated to be 89.12%.

B. *CDFIG simulation results*

The power machine stator current is shown in Fig. 13. The stator current and rotor speed of the CDFIG follow a similar pattern during transient periods compared to the DFIG. This is due to the fact that the same control is implemented on both CDFIG and DFIG.

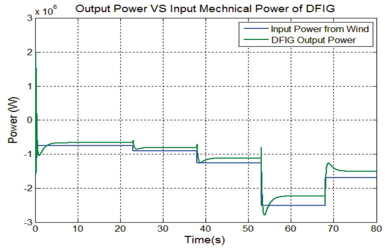

Fig. 12. The DFIG mechanical input and total output power.

The rotational speed of the CDFIG is indicated in Fig. 14. Since the CDFIG is essentially two IMs connected together through the rotor both mechanically and electrically, we only show the results for each individual machine. It can be seen that the rotor speed as well as the stator current are halved while producing the same power output. The input mechanical power and the total output are illustrated in Fig. 15. It is determined that the average efficiency of the CDFIG is 92.23%.

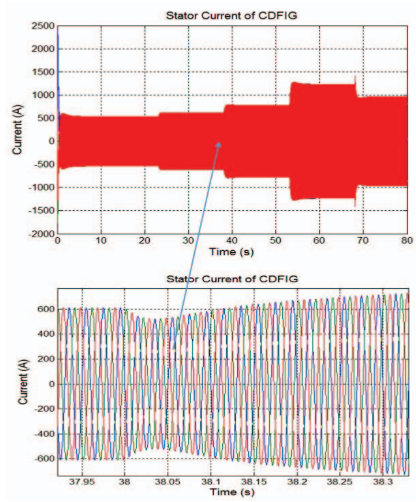

Fig. 13. The power machine stator current of CDFIG

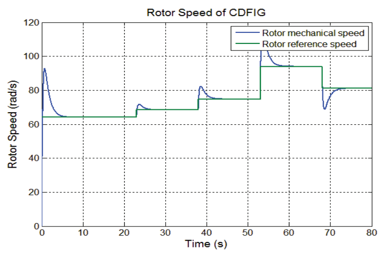

Fig. 14. The rotor speed of CDFIG

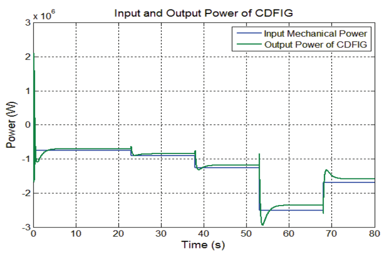

Fig. 15. The combined power of the CDFIG

VIII. Conclusion

A reference DFIG analytical design is employed and scaled. The reference and scaled DFIGs have similar dynamic behaviors due to scaling policy target. The analytical design is verified by Maxwell 2D. The machines have similar efficiencies and the CDFIG material cost is cheaper than DFIG. Then, the scaled machine's details are used to model a CDFIG. The WECS has been adjusted for the reference and scaled DFIGs. The WECSs are simulated by adapting CDFIG and DFIG models under an assumed wind profile. The improvement of the system efficiency with CDFIG is 3 percent. Although the CDFIG requires more investigation to overcome the control challenges, a large amount of energy will be saved in a large wind farm with the use of CDFIGs instead of DFIGs. If WECS overcomes to CDFIGs controlling issues, they can be drive gearless which will ultimately reduce the maintenance cost.

IX. References

[1] T. Shanker, R. K. Singh, and M. Ieee, "Wind Energy Conversion System : A Review," 2012.

[2] K. W. E. Cheng, J. K. Lin, Y. J. Bao, and X. D. Xue, "Review of the Wind Energy Generating System," 2011.

[3] A. Acakpovi and E. Ben Hagan, "A Wind Turbine System Model using a Doubly-Fed Induction Generator (DFIG)," *nternational J. Comput. Appl.*, vol. 90, no. 15, pp. 6–11, 2014.

[4] A. M. Alkandari, S. A. Soliman, and M. H. Abdel-rahman, "Steady State Analysis of a Doubly Fed Induction Generator," vol. 2011, no. September, pp. 393–400, 2011.

[5] P. Camocardi, P. Battaiotto, and R. Mantz, "Wind Generator with Double Stator Induction Machine. Control Strategy for a Water Pumping Application.," in *2008 43rd International Universities Power Engineering Conference*, 2008, pp. 1–5.

[6] B. Smith, "Theory and Performance of a Twin Stator Induction Machine," *IEEE Trans. Power Appar. Syst.*, vol. PAS-85, no. 2, pp. 123–131, Feb. 1966.

[7] D. Basic, Jian Guo Zhu, and G. Boardman, "Transient Performance Study of a Brushless Doubly Fed Twin Stator Induction Generator," *IEEE Trans. Energy Convers.*, vol. 18, no. 3, pp. 400–408, Sep. 2003.

[8] G. Boardman, J. G. Zhu, and Q. P. Ha, "Power flow in a doubly fed twin stator induction Machines," in *IEEE Conference on power System Technology*, 2000, pp. 99–104.

[9] M. Adamowicz and R. Strzelecki, "Cascaded Doubly Fed Induction Generator for mini and micro Power Plants Connected to Grid," in *2008 13th International Power Electronics and Motion Control Conference*, 2008, pp. 1729–1733.

[10] M. Adamowicz, R. Strzelecki, and P. Mysiak, "Cascaded Doubly Fed Induction Ggenerator using PFC Rectifiers," in *2009 Compatability and Power Electronics*, 2009, pp. 186–190.

[11] Vestast, "Vestas V100 2.5MW," *Most*, 2013. .

[12] Hui Li, Zhe Chen, and H. Polinder, "Optimization of Multibrid Permanent-Magnet Wind Generator Systems," *IEEE Trans. Energy Convers.*, vol. 24, no. 1, pp. 82–92, Mar. 2009.

[13] R. Harrison, E. Hau, and H. Snel, *Large wind turbines*. Wiley, 2000.

[14] A. D. Lilla, H. Dehnavifard, M. A. Khan, and P. Barendse, "Optimization of high voltage geared permanent-magnet synchronous generator systems," in *2014 International Conference on Electrical Machines (ICEM)*, 2014, pp. 1356–1362.

[15] J. Tamura, "Calculation Method of Losses and Efficiency of Wind Generators," in *WIND ENERGY CONVERSION SYSTEMS*, 2012, pp. 25–51.

[16] M. Fratila, A. Benabou, A. Tounzi, and M. Dessoude, "Calculation of Iron Losses in Solid Rotor Induction Machine Using FEM," *IEEE Trans. Magn.*, vol. 50, no. 2, pp. 825–828, 2014.

[17] H. Dehnavifard, A. D. Lilla, M. A. Khan, and P. Barendse, "Design and optimization of DFIGs with alternate voltage and speed ratings for wind applications," in *2014 International Conference on Electrical Machines (ICEM)*, 2014, pp. 2008–2013.

[18] R. Solomon, M. A. Khan, P. S. Barendse, P. Pillay, and K. A. Folly, "Review and Application of Micromachines for Wind Energy Integration," *IEEE Int. Conf. Electr. Mach.*, pp. 2151–2157, 2012.

[19] T. J. Hammons and A. J. Parsons, "Design of Microalternator for Power-System-Stability Investigations," *Proc. Inst. Electr. Eng. UK*, vol. 118, no. 10, p. 1421, 1971.

[20] M. J. Jefferies and A. Wright, "New Approach to Micromachine Construction," *Proc. Inst. Electr. Eng. UK*, vol. 117, no. 7, p. 1309, 1970.

[21] S. Berchten, K. Reichert, and E. Thaler, "Micromachine for Real-Time Generator Simulation Design Limits and a Novel Solution with Adjustable Parameters," *IEEE Trans. Energy Con.*, vol. 9, no. 12, pp. 38–39, 1989.

[22] T. A. Lipo, *Introduction to AC Machine Design*. Wisconsin Power Electronics Research Center, University of Wisconsin, 2004.

[23] H. Dehnavifard, M. A. Khan, and P. Barendse, "Development of a 5kW scaled prototype of a 2.5 MW Doubly-fed induction generator," in *2015 IEEE Energy Conversion Congress and Exposition (ECCE)*, 2015, pp. 990–996.

[24] Y. Lei, A. Mullane, G. Lightbody, and R. Yacamini, "Modeling of the Wind Turbine With a Doubly Fed Induction Generator for Grid Integration Studies," *IEEE Trans. Energy Convers.*, vol. 21, no. 1, pp. 257–264, Mar. 2006.

[25] K. Protsenko and Dewei Xu, "Modeling and Control of Brushless Doubly-Fed Induction Generators in Wind Energy Applications," *IEEE Trans. Power Electron.*, vol. 23, no. 3, pp. 1191–1197, May 2008.

[26] G. Esfandiari, M. Ebrahimi, A. Tabesh, and M. Esmaeilzadeh, "Dynamic Modeling and Analysis of Cascaded DFIMs in an Arbitrary Reference Frame," pp. 1–9, 2015.

[27] G. Boukettaya, O. Naifar, and A. Ouali, "A vector Control of a Cascaded Doubly Fed Induction Generator for a Wind Energy Conversion System," in *2014 IEEE 11th International Multi-Conference on Systems, Signals & Devices (SSD14)*, 2014, pp. 1–7.

[28] D. Picovici, D. Levy, A. Mahdi, and T. Coffey, "The Cascade Induction Machine: A Reliable and Controllable Motor or Generator," *Elect. Power Syst. Res.*, vol. 68, no. 3, pp. 193–207, 2004.

[29] N. Patin, E. Monmasson, and J.-P. Louis, "Modeling and Control of a Cascaded Doubly Fed Induction Generator Dedicated to Isolated Grids," *IEEE Trans. Ind. Electron.*, vol. 56, no. 10, pp. 4207–4219, Oct. 2009.

X. Biography

H. Dehnavifard was born in Tehran, Iran in 1985. He completed his Bachelor's and Master degrees in Electrical Engineering at Amirkabir University of Technology, Tehran in 2008 and 2011 respectively. He came to South Africa to pursue his PhD in Electrical Engineering at the University of Cape Town in 2013. He is currently a 4th year PhD candidate and intends to submit his thesis in June 2016. His research interests are electrical power systems, electrical machine design, renewable energy, semiconductor gas sensor, and RFID.

X. M. Hu was born in Johannesburg, South Africa in 1992. He completed his Bachelor's degree in Electrical Engineering at University of Cape Town, Cape Town in 2014. Since 2015, he has been in progress with his Master's degree in electrical engineering in the University of Cape Town. His research interests are electrical power systems, renewable energy, machine control and modulation of converters.

M. A. Khan received the B.Sc. (Eng.), M.Sc., and Ph.D. degrees in electrical engineering from the University of Cape Town in South Africa. He is currently an Associate Professor at the University of Cape Town, where his research interests include electrical machines, drives and renewable energy systems.

P. S. Barendse received the B.Sc. (Eng.), M.Sc., and Ph.D. degrees in electrical engineering from the University of Cape Town in South Africa. He is currently an Associate Professor at the University of Cape Town. His research interests include condition monitoring, drives, fuel cells, and energy efficiency.